JACS
JOURNAL OF THE AMERICAN CHEMICAL SOCIETY
Communication
pubs.acs.org/JACS

Metal-Cluster-Sensitized Solar Cells. A New Class of Thiolated Gold Sensitizers Delivering Efficiency Greater Than 2%

Yong-Siou Chen,[†] Hyunbong Choi,[†] and Prashant V. Kamat*

Radiation Laboratory and Department of Chemistry and Biochemistry, University of Notre Dame, Notre Dame, Indiana 46556, United States

Supporting Information

ABSTRACT: A new class of metal-cluster sensitizers has been explored for designing high-efficiency solar cells. Thiol-protected gold clusters which exhibit molecular-like properties have been found to inject electrons into TiO_2 nanostructures under visible excitation. Mesoscopic TiO_2 films modified with gold clusters deliver stable photocurrent of 3.96 mA/cm^2 with power conversion efficiencies of 2.3% under AM 1.5 illumination. The overall absorption features and cell performance of metal-cluster-sensitized solar cells (MCSCs) are comparable to those of CdS quantum-dot-based solar cells (QDSCs). The relatively high open-circuit voltage of 832 mV and fill factor of 0.7 for MCSCs as compared to QDSCs show the viability of these new sensitizers as alternatives to semiconductor QDs and sensitizing dyes in the next generation of solar cells. The superior performance of MCSCs discussed in this maiden study lays the foundation to explore other metal clusters with broader visible absorption.

Catalytic and plasmonic properties make noble metal nanoparticles (NPs) valuable building blocks for designing energy conversion and sensing devices.[1] For example, metal NPs have been successfully employed as electrocatalysts in fuel cells, cocatalysts in photocatalytic water-splitting reactions, and plasmonic particles in surface-enhanced Raman spectroscopy. Recently, many reports have indicated silver and gold NPs to be photoactive in the visible as they participate in electron-transfer reactions.[2] In many cases photocurrent generation or water-splitting reaction has been presented as the support for the visible-light-induced electron-transfer process. Surface plasmon resonance has often been cited as the reason for such visible activity.[3] However, mechanistic evidence that directly supports electron transfer arising from plasmon excitation remains elusive.

In recent years, a new class of nanomaterials has emerged: few-metal-atom clusters that are protected by thiolate ligands are now well characterized.[4] Many of these metal clusters, which were identified as weakly emitting NPs nearly a decade ago, have now been explored as metallic clusters with molecular-like properties.[5] Thiolate groups such as 2-phenylethanethiolate (SR) have been found to control the number of metal atoms and ligands in a stabilized metal cluster. Of particular interest are $Au_{144}(SR)_{60}$, $Au_{102}(SR)_{44}$, $Au_{38}(SR)_{24}$, and $Au_{25}(SR)_{18}$ clusters whose structures have been well characterized using crystallography, mass spectrometry, and computational methods.[4d,6] Similarly, $(Ag)_8$ clusters protected with dihydrolipoic acid (DHLA) have been shown to exhibit photoinduced electron-transfer properties.[7] Thiolate-capped gold and silver metal clusters exhibit high fluorescence quantum yields ($\varphi_f > 0.1$). Our recent results have shown that a metallic core capped with a metal cluster shell of $(Ag)_8$-DHLA is highly emissive in the visible region.[7b] In another recent study, L-glutathione was employed as the complexing ligand which further induced reduction of Au(III) and produced luminescent Au(0)@Au(I)-thiolate clusters with φ as high as 0.15.[8]

It has also been questioned whether many metal particles that exhibit visible photoactivity have surfaces that are decorated with photoactive metal clusters in a core@shell morphology.[2a,7b] Earlier studies employing glutathione-protected gold clusters attached to TiO_2 reported relatively low external quantum efficiencies (5−15%).[9] The photocurrents recorded in the visible are usually in the range of nA−μA. The molecular-like properties of such metal clusters make them suitable sensitizers for capture and conversion of incident photons in solar cells. We now have successfully modified mesoscopic TiO_2 films with Au clusters stabilized with L-glutathione and manipulated the charge injection from its excited state into TiO_2 NPs. The excited-state interactions and delivery of stable photocurrent in metal-cluster-sensitized solar cells (MCSCs) are discussed.

Scheme 1. Schematic Illustration of the Working Principle of a Metal-Cluster-Sensitized Solar Cell

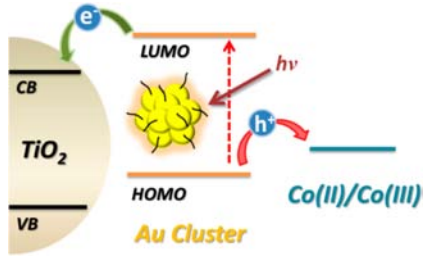

Excited-State Interaction with TiO_2 Colloids. The L-glutathione-protected metal clusters were synthesized using a literature method.[8] Small clusters having a few-gold-atom core capped with a Au-thiolate shell were formed as the solution aged for 24 h. In the present study we refer to these clusters as Au_x-SH. The experimental details and evolution of absorption and

Received: April 16, 2013
Published: May 29, 2013

   dx.doi.org/10.1021/ja403807f | J. Am. Chem. Soc. 2013, 135, 8822−8825

emission features during the 24 h aging process are presented in the Supporting Information (Figure S1).

No additional changes were observed after 24 h, and these spectral features remained stable for several days. These Au_x-SH clusters showed absorption below 525 nm with a characteristic absorption shoulder around 400 nm (Figure 1A). Luo et al.

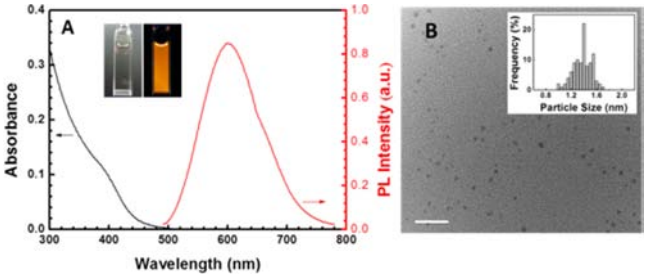

Figure 1. (A) Absorption and emission spectra of L-glutathione-protected metal clusters in water. The spectra were recorded after 24 h. (B) TEM image and particle size distribution histogram. Scale bar, 10 nm. Inset in (A): photographs of Au_x-SH in H_2O under room light (left) and UV light (right).

identified these clusters as Au(0)@Au(I)-thiolate structures with relatively high concentration of thiolate ligand (1:1 ratio of Au:thiolate) in the shell.[8] It should be noted that Au_{25}-glutathione clusters employed by Tatsuma's group[9a] had different absorption features (absorption up to 700 nm) and excited-state energetics than the Au_x-glutathione clusters. These absorption variations highlight the difference in the HOMO–LUMO transitions of these two types of clusters.

The transmission electron micrograph (Figure 1B) shows very small particles with diameters of 1.0–1.6 nm, in agreement with earlier studies which reported similar dimensions for L-glutathione-complexed Au clusters.[8] Using MS analysis, those researchers characterized them as clusters having >29 gold atoms.

The Au_x-SH clusters prepared in our study exhibit orange emission which can be readily visualized under UV light (Figure 1A). The increase in the emission yield (Figure S1B) with time of aging parallels the increase seen in the absorption and stabilizes after ~24 h. The emission maximum at 600 nm represents excited-state deactivation of these Au clusters via a radiative route. As discussed in earlier studies, such characteristic emission of Au and Ag clusters represents molecular-like properties.[7,10] The emission quantum yield of 0.02 for Au clusters is relatively low. The emission quantum yield in the present study was measured using $Ru(bpy)_3^{2+}$ as the reference.

Figure 2 shows the quenching of Au metal cluster emission by TiO_2 colloids. Known amounts of TiO_2 colloids were added into the Au_x-SH cluster suspension, and emission spectra were recorded. Increasing TiO_2 concentrations led to a decrease of emission, suggesting that an additional pathway is responsible for deactivating excited Au_x-SH. At >150 μM TiO_2 (concentration expressed in terms molecules), we see total quenching of the emission. As shown earlier, interaction between a sensitizer and TiO_2 colloid can be analyzed by considering an equilibrium between the two with an apparent association constant of K_{app}:[11]

$$Au_x\text{-SH} + TiO_2 \rightleftarrows (Au_x\text{-SH}\cdots TiO_2) \quad (1)$$

The observed decrease in the emission yield ($\varphi^0 - \varphi_{obsd}$) can be related to the TiO_2 concentration using the expression

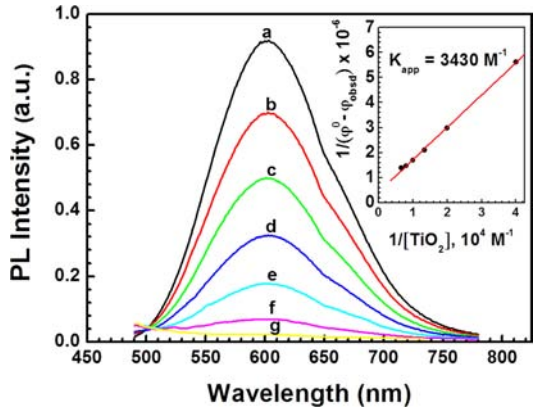

Figure 2. Emission spectra of Au_x-SH solution containing different concentrations of TiO_2: (a) 0, (b) 25, (c) 50, (d) 75, (e) 100, (f) 125, and (g) 150 μM. Excitation wavelength = 400 nm. Inset: Dependence of $1/(\varphi^0 - \varphi_{obsd})$ on the reciprocal concentration of TiO_2.

$$1/(\varphi^0 - \varphi_{obsd}) = 1/(\varphi^0 - \varphi') + 1/K_{app}(\varphi^0 - \varphi')[TiO_2] \quad (2)$$

The linearity of the double reciprocal plot shows the validity of this analysis. From the slope of this plot we obtain an apparent association constant of 3430 M^{-1}. The strong interaction between the two is attributed to the charge injection from excited Au_x-SH into the conduction band of TiO_2,

$$(Au_x\text{-SH}^*\cdots TiO_2) \rightarrow (Au_x\text{-SH})^+ + TiO_2(e) \quad (3)$$

It is interesting to note that the energy gap between the ground and excited states of Au_x-SH clusters (HUMO–LUMO gap) as measured from the absorption onset (525 nm) is ~2.36 eV. However, the emission maximum at 600 nm suggests a lower relaxed energy state (energy gap of 2 eV) is responsible for the stabilizing the excited state. Such an excited state, likely the result of ligand-to-metal charge transfer[8] within the Au_x-SH, is responsible for the charge injection process.

Photosensitization of TiO_2 Films. If indeed the charge injection process illustrated in reaction 3 is reasonably efficient, we should be able to drive the electrons from TiO_2 to generate photocurrent in a photoelectrochemical cell. The expected mechanism is similar to those of dye-sensitized and quantum-dot-sensitized solar cells.[12] The mesoscopic films of TiO_2 were first cast on fluorine-doped tin oxide (FTO) glass electrodes. These electrodes were immersed in the Au_x-SH cluster solutions for 48 h. Significant binding of Au clusters to the TiO_2 surface was noticed from the changes in the absorption (Figure S2). The Au_x-SH clusters adsorbed on TiO_2 exhibited the characteristic absorption below 525 nm. We sandwiched the Au-cluster-modified TiO_2 electrode with Pt-deposited FTO counter electrode separated by a 50 μm spacer. A redox electrolyte of $Co(bpy)_3(PF_6)_2/Co(bpy)_3(PF_6)_3$ was introduced between the two electrodes. The performance of the resulting photoelectrochemical cell was tested under AM 1.5 simulated solar irradiation.

Photocurrent action spectra of the MCSC consisting of a Au_x-SH-modified TiO_2 mesoscopic film as the photoanode were recorded using monochromatic light irradiation. The external quantum efficiency or incident photon to photocurrent generation efficiency (IPCE) of the MCSC is presented in Figure 3. The photoanode is responsive below 525 nm and matches well with the absorption of Au_x-SH clusters. These results confirm that the photocurrent indeed comes from the

dx.doi.org/10.1021/ja403807f | J. Am. Chem. Soc. 2013, 135, 8822–8825

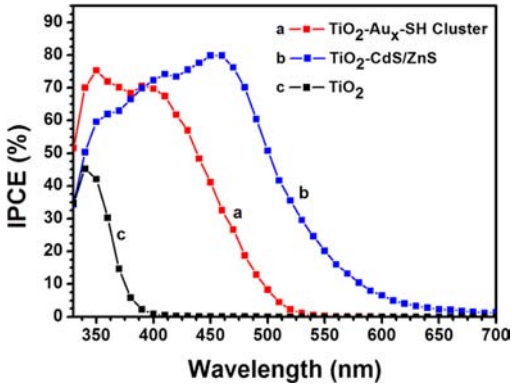

Figure 3. IPCE spectra (external quantum efficiency) of photoelectrochemical cell using photoanodes composed of (a) TiO_2–Au_x-SH cluster, (b) TiO_2–CdS/ZnS, and (c) TiO_2. Traces (a) and (c) were recorded using 0.22 M $Co(bpy)_3(PF_6)_2$, 0.033 M $Co(bpy)_3(PF_6)_3$, 0.1 M $LiClO_4$, and 0.5 M 4-*tert*-butylpyridine in acetonitrile as electrolyte and Pt deposited on FTO as counter electrode. Trace (b) was recorded using 2 M Na_2S and 2 M S in H_2O as electrolyte and Cu_2S-RGO film deposited on FTO as counter electrode.

excitation of Au_x-SH metal clusters. The maximum IPCE of 70% observed at 400–425 nm shows that we are able to capture the incident photons and convert them to electrical energy quite efficiently. We also prepared a quantum dot solar cell (QDSC) using a CdS/ZnS-modified TiO_2 electrode using the SILAR method and a Cu_2S/graphene oxide counter electrode with a S_2^{-}/S_n^{2-} redox electrolyte.[13] Since CdS has absorption similar to that of Au_x-SH clusters in the visible (350–550 nm), we compared the performance of these two photoelectrochemical solar cells. Interestingly, the observed IPCE of MCSC is close to that of high-efficiency (80%) CdS QDSC. If we employ Co(II)/Co(III) redox couple instead of S_2^{-}/S_n^{2-}, we observe lower photovoltaic performance (efficiency ~1%) with CdS photoanode (Table 1 and Figure S3).[14] Although the Au_x-SH clusters

Table 1. Photovoltaic Performance of Solar Cells

sensitizer	J_{sc} (mA cm^{-2})	V_{oc} (V)	*ff*	η (%)
Au_x-SH 1[a]	3.96	0.832	0.716	2.36
Au_x-SH 2[a]	3.50	0.825	0.701	2.03
Au_x-SH 3[a]	3.70	0.827	0.678	2.07
Au_x-SH 4[a]	3.82	0.809	0.681	2.11
Au_x-SH 5[a]	3.81	0.820	0.687	2.13
CdS[b]	2.34	0.704	0.620	1.01
CdS/ZnS[c]	7.52	0.537	0.579	2.34
None (TiO_2)	0.11	0.279	0.454	0.013

[a]Performance of five different Au_x-SH sensitized TiO_2 solar cells were measured using 0.15–0.20 cm^2 exposed area with shadow mask under AM 1.5 illumination. Electrolyte: 0.22 M $Co(bpy)_3(PF_6)_2$, 0.033 M $Co(bpy)_3(PF_6)_3$, 0.1 M $LiClO_4$, and 0.5 M 4-*tert*-butylpyridine in acetonitrile. Counter electrode: Pt. *ff* and η correspond to fill factor and power conversion efficiency, respectively. [b]From ref 14 (using Co(II)/Co(III) redox couple). [c]Electrolyte: 2 M Na_2S, 2 M S in H_2O. Counter electrode: Cu_2S-RGO.

are able to generate photocurrent with 70% efficiency in the 400–425 nm region, the lack of absorbance at wavelengths above 525 nm makes them nonresponsive to the entire visible spectrum.

MCSC versus QDSC. We further evaluated the performance of the MCSC by recording the *J*–*V* characteristics (Figure 4A).

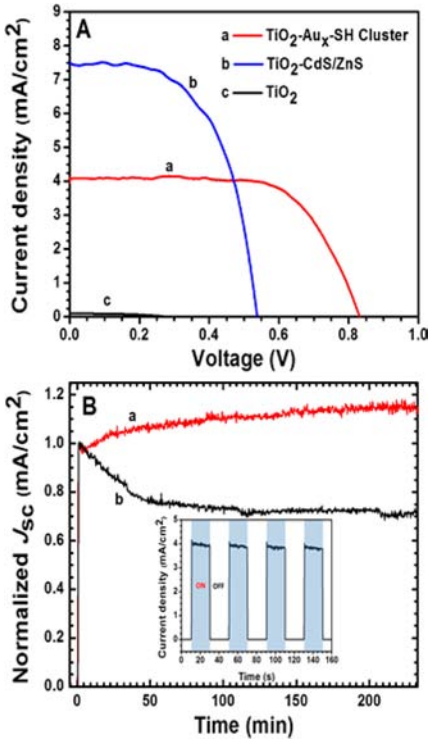

Figure 4. (A) *J*–*V* characteristics and (B) photocurrent stability of MCSC and QDSC employing photoanodes: (a) TiO_2 modified with Au_x-SH cluster, (b) TiO_2 modified with CdS/ZnS, and (c) TiO_2 under steady-state illumination of 100 mW/cm^2. The photocurrents using two cells were normalized to the value recorded immediately after illumination. Inset in (B) shows the photocurrent response to on/off cycles of illumination of a photoelectrochemical cell with TiO_2 modified with Au_x-SH as anodes. The redox electrolyte and counter electrode were the same as in Figure 3.

An open-circuit voltage (V_{oc}) of 832 mV and short-circuit current (J_{sc}) of 3.96 mA/cm^2 show the effectiveness of the Au_x-SH cluster in converting light energy into electrical energy. The fill factor of the MCSC (*ff* = 0.7) which was obtained from the *J*–*V* characteristics in turn confirms the effective operation of MCSC and exemplifies the role of Co(II)/Co(III) as an effective redox couple. The observed V_{oc} is among the highest measured for liquid junction solar cells. We have prepared several solar cells using TiO_2/Au_x-SH as the photoanode and evaluated their performance to test the role of Au_x-SH as the effective sensitizer as well as the reproducibility of the MCSC design. The performance of five representative MCSCs is summarized in Table 1.

Maximum power conversion efficiency (η) in the range of 2.03–2.36% was observed in these MCSCs. The maximum η reported with CdS QDs is ~2.34%. Similar efficiency values in the range of 2–3% have been noted for CdS-based QDSCs.[15] It is interesting to note that the observed *ff* and η values are comparable (or even slightly superior) to those obtained with QDSC employing CdS/ZnS photoanodes under the present experimental conditions. More interestingly, the V_{oc} and *ff* of the Au_x-SH-sensitized solar cell are comparable to those of dye-sensitized solar cells (DSSCs). The only difference between DSSCs and MCSCs employed in the present study is the partial absorption of incident visible photons by Au_x-SH, which seems to limit the net power conversion efficiency. We also determined the stability of the photocurrent generation in MCSC employing Au_x-SH photoanode and compared it with that of CdS/ZnS

dx.doi.org/10.1021/ja403807f | J. Am. Chem. Soc. 2013, 135, 8822–8825

photoanode in QDSC (Figure 4B). The photocurrent generation in MCSC is prompt, as indicated by its response to incident white light irradiation. When subjected to long-term irradiation, Au_x-SH-modified TiO_2 photoanode exhibited a small increase in the photocurrent as a result of light-soaking effects. Following this initial increase, the photocurrent generation stabilized and remained steady during the rest of the continuous illumination period (4 h). On the other hand, QDSC employing CdS/ZnS photoanode exhibited a small decrease initially but remained steady during the rest of the illumination. These results clearly highlight the photostability of Au_x-SH clusters in the presence of Co(II)/Co(III) regenerative redox couple.

In summary, the ability of Au_x-SH metal clusters to serve as a new class of photosensitizers in mesoscopic TiO_2-based solar cells has been successfully identified. This maiden effort of using thiolated metal clusters in solar cells opens up new opportunities to explore photosensitizing properties in other light energy conversion devices. Au_x-SH cluster employed in this investigation has a Au(0) core@Au(I)-thiolate shell structure which is different than those used in earlier attempts to employ them as sensitizers. The higher energy HUMO/LUMO gap and stronger interaction with TiO_2 allow effective electron injection, as evidenced by higher photovoltage. The Co(II)/Co(III) couple enables the delivery of the steady photocurrent. The relatively high power conversion efficiency (>2%) achieved in the present study sets a major landmark for recognizing important photoactivity of thiolated metal clusters. If the absorption of ligand-stabilized metal clusters can be further extended into the red−infrared region, we can expect significant enhancement in power conversion efficiencies. The Au_x-SH clusters employed in the present study have limited absorption in the visible. However, opportunities exist to couple these metal clusters with plasmonic metal nanoparticles and further increase the absorption range of the MCSCs. Efforts are underway to explore these effects cooperatively in DSSCs and QDSCs by introducing metal-cluster-capped gold and silver nanoparticles. Such studies should enable distinguishing plasmonic effect and metal cluster sensitization effects in solar cells.

■ ASSOCIATED CONTENT

Ⓢ Supporting Information

Experimental methods; absorption and emission spectra; and *J*−*V* plots. This material is available free of charge via the Internet at http://pubs.acs.org.

■ AUTHOR INFORMATION

Corresponding Author

pkamat@nd.edu

Author Contributions

†Y.-S.C. and H.C. contributed equally to this work.

Notes

The authors declare no competing financial interest.

■ ACKNOWLEDGMENTS

The research described herein was supported by the Division of Chemical Sciences, Geosciences and Biosciences, Basic Energy Sciences, Office of Science, U.S. Department of Energy through grant no. DE-FC02-04ER15533. H.C. acknowledges support from the University of Notre Dame SAPC program. This is contribution no. NDRL 4972 from the Notre Dame Radiation Laboratory.

■ REFERENCES

(1) (a) Kamat, P. V. *J. Phys. Chem. Lett.* **2012**, *3*, 663. (b) Hägglund, C.; Apell, S. P. *J. Phys. Chem. Lett.* **2012**, *3*, 1275. (c) Ferry, V. E.; Munday, J. N.; Atwater, H. A. *Adv. Mater.* **2010**, *22*, 4794. (d) Osterloh, F. E. *Chem. Soc. Rev.* **2013**, *42*, 2294. (e) Stratakis, M.; Garcia, H. *Chem. Rev.* **2012**, *112*, 4469. (f) Choi, H.; Chena, W. T.; Kamat, P. V. *ACS Nano* **2012**, *6*, 4418. (g) Takai, A.; Kamat, P. V. *ACS Nano* **2011**, *4*, 7369.

(2) (a) Diez, I.; Ras, R. H. A. *Nanoscale* **2011**, *3*, 1963. (b) Thimsen, E.; Le Formal, F.; Gratzel, M.; Warren, S. C. *Nano Lett.* **2011**, *11*, 35.

(3) (a) Awazu, K.; Fujimaki, M.; Rockstuhl, C.; Tominaga, J.; Murakami, H.; Ohki, Y.; Yoshida, N.; Watanabe, T. *J. Am. Chem. Soc.* **2008**, *130*, 1676. (b) Kulkarni, A. P.; Noone, K. M.; Munechika, K.; Guyer, S. R.; Ginger, D. S. *Nano Lett.* **2010**, *10*, 1501. (c) Standridge, S. D.; Schatz, G. C.; Hupp, J. T. *J. Am. Chem. Soc.* **2009**, *131*, 8407. (d) Thomann, I.; Pinaud, B. A.; Chen, Z.; Clemens, B. M.; Jaramillo, T. F.; Brongersma, M. L. *Nano Lett.* **2011**, *11*, 3440. (e) Salvador, M.; MacLeod, B. A.; Hess, A.; Kulkarni, A. P.; Munechika, K.; Chen, J. I. L.; Ginger, D. S. *ACS Nano* **2012**, *6*, 10024. (f) Nishijima, Y.; Ueno, K.; Yokota, Y.; Murakoshi, K.; Misawa, H. *J. Phys. Chem. Lett.* **2010**, *1*, 2031. (g) Nabika, H.; Takase, M.; Nagasawa, F.; Murakoshi, K. *J. Phys. Chem. Lett.* **2010**, *1*, 2470.

(4) (a) Negishi, Y.; Chaki, N. K.; Shichibu, Y.; Whetten, R. L.; Tsukuda, T. *J. Am. Chem. Soc.* **2007**, *129*, 11322. (b) Parker, J. F.; Fields-Zinna, C. A.; Murray, R. W. *Acc. Chem. Res.* **2010**, *43*, 1289. (c) Jin, R.; Qian, H.; Wu, Z.; Zhu, Y.; Zhu, M.; Mohanty, A.; Garg, N. *J. Phys. Chem. Lett.* **2010**, *1*, 2903. (d) Negishi, Y.; Sakamoto, C.; Ohyama, T.; Tsukuda, T. *J. Phys. Chem. Lett.* **2012**, *3*, 1624. (e) Aikens, C. M.; Li, S. Z.; Schatz, G. C. *J. Phys. Chem. C* **2008**, *112*, 11272.

(5) (a) Link, S.; Beeby, A.; FitzGerald, S.; El-Sayed, M. A.; Schaaff, T. G.; Whetten, R. L. *J. Phys. Chem. B* **2002**, *106*, 3410. (b) Wu, Z. K.; Jin, R. C. *Nano Lett.* **2010**, *10*, 2568.

(6) (a) Bahena, D.; Bhattarai, N.; Santiago, U.; Tlahuice, A.; Ponce, A.; Bach, S. B. H.; Yoon, B.; Whetten, R. L.; Landman, U.; Jose-Yacaman, M. *J. Phys. Chem. Lett.* **2013**, *4*, 975. (b) Whetten, R. L.; Khoury, J. T.; Alvarez, M. M.; Murthy, S.; Vezmar, I.; Wang, Z. L.; Stephens, P. W.; Cleveland, C. L.; Luedtke, W. D.; Landman, U. *Adv. Mater.* **1996**, *8*, 428. (c) Whetten, R. L.; Price, R. C. *Science* **2007**, *318*, 407. (d) Jin, R. C. *Nanoscale* **2010**, *2*, 343. (e) Zhu, M.; Qian, H.; Jin, R. *J. Phys. Chem. Lett.* **2010**, *1*, 1003. (f) Tang, Z. H.; Robinson, D. A.; Bokossa, N.; Xu, B.; Wang, S. M.; Wang, G. L. *J. Am. Chem. Soc.* **2011**, *133*, 16037. (g) Shichibu, Y.; Negishi, Y.; Tsukuda, T.; Teranishi, T. *J. Am. Chem. Soc.* **2005**, *127*, 13464. (h) Kurashige, W.; Yamaguchi, M.; Nobusada, K.; Negishi, Y. *J. Phys. Chem. Lett.* **2012**, *3*, 2649.

(7) (a) Rao, T. U. B.; Pradeep, T. *Angew. Chem., Int. Ed.* **2010**, *49*, 3925. (b) Chen, W.-T.; Hsu, Y.-J.; Kamat, P. V. *J. Phys. Chem. Lett.* **2012**, *3*, 2493.

(8) Luo, Z. T.; Yuan, X.; Yu, Y.; Zhang, Q. B.; Leong, D. T.; Lee, J. Y.; Xie, J. P. *J. Am. Chem. Soc.* **2012**, *134*, 16662.

(9) (a) Sakai, N.; Tatsuma, T. *Adv. Mater.* **2010**, *22*, 3185. (b) Kogo, A.; Sakai, N.; Tatsuma, T. *Nanoscale* **2012**, *4*, 4217.

(10) (a) Zheng, J.; Nicovich, P. R.; Dickson, R. M. *Annu. Rev. Phys. Chem.* **2007**, *58*, 409. (b) Zheng, J.; Dickson, R. M. *J. Am. Chem. Soc.* **2002**, *124*, 13982.

(11) Kamat, P. V. *J. Phys. Chem.* **1989**, *93*, 859.

(12) (a) Peter, L. M. *J. Phys. Chem. Lett.* **2011**, *2*, 1861. (b) Yella, A.; Lee, H.-W.; Tsao, H. N.; Yi, C.; Chandiran, A. K.; Nazeeruddin, M. K.; Diau, E. W.-G.; Yeh, C.-Y.; Zakeeruddin, S. M.; Grätzel, M. *Science* **2011**, *334*, 629. (c) Hetsch, F.; Xu, X.; Wang, H.; Kershaw, S. V.; Rogach, A. L. *J. Phys. Chem. Lett.* **2011**, *2*, 1879. (d) Kamat, P. V. *J. Phys. Chem. Lett.* **2013**, *4*, 908. (e) Toyoda, T.; Shen, Q. *J. Phys. Chem. Lett.* **2012**, *3*, 1885.

(13) Radich, J. G.; Dwyer, R.; Kamat, P. V. *J. Phys. Chem. Lett.* **2011**, *2*, 2453.

(14) Choi, H.; Nicolaescu, R.; Paek, S.; Ko, J.; Kamat, P. V. *ACS Nano* **2011**, *5*, 9238.

(15) (a) Santra, P. K.; Nair, P. V.; Thomas, K. G.; Kamat, P. V. *J. Phys. Chem. Lett.* **2013**, *4*, 722. (b) Li, L.; Yang, X. C.; Gao, J. J.; Tian, H. N.; Zhao, J. Z.; Hagfeldt, A.; Sun, L. C. *J. Am. Chem. Soc.* **2011**, *133*, 8458.